Latin American Journal of Solids and Structures
www.lajss.org

Nonlinear Dynamics Analysis of FGM Shell Structures with a Higher Order Shear Strain Enhanced Solid-Shell Element

Abstract

In this paper, non-linear dynamics analysis of functionally graded material (FGM) shell structures is investigated using the higher order solid-shell element based on the Enhanced Assumed Strain (EAS). With this element, a quadratic distribution of the shear stress through the thickness is considered in an enhancing part. Material properties of the shell structure are varied continuously in the thickness direction according to the general four-parameter power-law distribution in terms of the volume fractions of the constituents. Performance and accuracy of the present higher order solid-shell element are confirmed by comparing the numerical results obtained from finite element analyses with results from the literature.

Keywords

Non-linear dynamics, Higher Order Shear Deformation, Shear locking, Solid-shell element, FGM.

A. Hajlaoui [a]
E. Triki [a]
A. Frikha [a]
M. Wali [a]
F. Dammak [a]

[a] Mechanical Modeling and Manufacturing Laboratory (LA2MP), National Engineering School of Sfax, B.P W3038, Sfax, University of Sfax, Tunisia
abdhajlaoui@gmail.com; emna_triki@yahoo.fr; frikhaahmed@yahoo.fr; mondherwali@yahoo.fr; fakhreddine.dammak@enis.rnu.tn

http://dx.doi.org/10.1590/1679-78253323

Received 26.08.2016
In revised form 26.10.2016
Accepted 06.11.2016
Available online 07.11.2016

1 INTRODUCTION

In the last decades, functionally graded materials (FGM) are becoming more widely used since they provide many advantages to structural designers. FGMs shell structures are widely used in aircraft and space systems due to their advantages of high stiffness and their high heat-resistance. In an FGM, the structure is prepared from a mixture of ceramic and metal, or a combination of other metals or other ceramics that are appropriate to achieve the desired objective. Material properties of

FGMs are varied continuously in one or more directions. Therefore, the stress distributions are smooth hence interface problems are eliminated when compared to laminate structure

In order to avoid structural failure caused by dynamic loadings, linear dynamic characteristics of FGMs shell structures have been considered by many researchers. Finding analytic solutions for linear and non-linear dynamics analysis of functionally graded material is a very difficult task, and they only exist for particular cases. Meanwhile, the finite-element (FE) method has become the most widely used technique to model the processes of dynamics analysis.

There are several solution formulations for vibration and linear dynamic analysis of FGM shells structures. They can be classified into two groups: the 2D plate and shell models and the full 3D elasticity model. Zhi-Yuan and Hua-Ning (2007) studied free vibration characteristics of functionally graded cylindrical shells with holes using Kirchhoff Classical thin Plate Theory (CPT). On the other hand, Kadoli and Ganesan (2006) studied the buckling and free vibration analysis of functionally graded cylindrical shells subjected to a temperature-specified boundary condition. In their analysis, the finite element equations based on the First order Shear Deformation Theory (FSDT) and the Plane Stress Assumption (PSA) were formulated. Recently, Ansari et al. (2016) developed a non-classical size-dependent plate model based on the modified strain gradient and the FSDT for the bending, buckling and free vibration analyses of microscale FG plates.

Based on the Third order Shear Deformation Theory (TSDT) and PSA, Reddy (2000) presented a theoretical formulation, Navier's solutions of rectangular plates, and finite element models to study the nonlinear dynamic response of FGM plates subjected to a suddenly applied uniform pressure. Yang and Shen (2002) analyzed free and forced vibration for initially stressed FGM plates. In this contribution, theoretical formulations are based on TSDT and PSA including the thermal effects. One-dimensional differential quadrature technique and Galerkin approach are used to determine the transient response of the plate subjected to dynamic loads. Gharooni and Ghannad (2015) investigated displacements and stresses in pressurized thick FGM cylinders with exponential variation of material properties based on TSDT. Furthermore, based on a TSDT of shells and PSA, Wali et al. (2015) Frikha et al. (2016) and Frikha et al. (2017) studied respectively the free vibration, linear dynamic response and fully geometrical nonlinear mechanical response of FGM shell structures using an efficient double directors shell element proposed in Wali et al. (2014). The shear stress boundary conditions on top and bottom faces are considered in a discrete form as given in (2005).

For full 3D elasticity formulations for vibration and linear dynamic analysis of FGM shells, one find the work of Vel and Batra (2004) based on three dimensional exact solutions for free and forced vibrations of simply supported FGM rectangular plates. In Asemi et al. (2014) the static and dynamic analyses of FGM skew plates are obtained based on the three-dimensional theory of elasticity. Graded elements, the principle of minimum energy and Rayleigh-Ritz energy method are used. Using 3D elasticity model, Nguyen and Nguyen-Xuan (2015) proposed an efficiently computational tool based on an isogeometric finite element formulation for static and dynamic response analysis of FGM plates.

Regarding the nonlinear dynamics analysis of FGM shells, three kinematics assumption are used, CPT, FSDT and TSDT.

Based on the CPT assumption and von-Karman geometrical nonlinearity, Woo et al. (2006) investigated the nonlinear free vibration behavior of FGM plates. Allahverdizadeh et al. (2008) evaluated the material properties of an FGM thin circular plate and investigated the nonlinear free and forced vibrations using the shooting technique. The formulation is based on CPT and von-Karman geometrical nonlinearity. Alijani et al. (2011) studied the nonlinear vibrations of FGM doubly curved shallow shells. They considered the thermal effect, the CPT assumption and Donnell nonlinearity. Using the CPT with an improved Donnell equations and PSA, Bich and Nguyen (2012) examined the nonlinear vibration of functionally graded circular cylindrical shells. Considering the CPT with PSA and von-Karman geometrical nonlinearity, Duc (2013) presented an analytic investigation on the nonlinear dynamic response of eccentrically stiffened functionally graded double curved shallow shells resting on elastic foundations and being subjected to axial compressive load and transverse load. Using the same considerations, Duc and Cong (2015) investigated the nonlinear dynamic response of imperfect symmetrical thin FGM plate on elastic foundation.

Using the FSDT plate finite element method with PSA employing von-Karman nonlinearity, Praveen and Reddy (1998) investigated the nonlinear transient thermo-elastic response of FGM plates. Liew et al. (2006) studied the nonlinear vibration of a coating-FGM-substrate cylindrical panel subjected to a temperature gradient. The FSDT is considered with PSA and von-Karman geometrical nonlinearity. Also based on the FSDT with PSA and von-Karman geometrical nonlinearity, Zhang et al. (2012) analyzed the nonlinear dynamics of a clamped–clamped FGM circular cylindrical shell subjected to an external excitation and uniform temperature change.

Based on TSDT and PSA, Hao et al. (2008) presented an analysis of the nonlinear dynamics of a simply supported FGM rectangular plate subjected to the transversal and in-plane excitations in a thermal environment. The von-Karman geometrical nonlinearity assumption is used. Using the same von-Karman geometrical nonlinearity with TSDT and PSA, Duc et al. (2015) presented an analytical approach to investigate the nonlinear dynamic response and vibration of imperfect FGM thick circular cylindrical shells surrounded on elastic foundation. Based on TSDT with PSA and von-Karman type nonlinear kinematics, Liu et al. (2015) presented a nonlinear dynamic analysis of a slightly initial imperfect FGM circular cylindrical shell subjected to complex loads including aerodynamic pressure and thermal loading.

It can be seen from the previous literature that in most of the studies, full 3D elasticity formulations are only limited to linear dynamic and free vibration of FGM structures. Also, the von-Karman or Donell geometrical nonlinearity are the only kinematic that has been basically used for the nonlinear dynamic analysis of shell's structures where the PSA is largely considered.

However, in this paper we focus on the fully 3D non-linear dynamics analysis of FGM shell structures by using higher order shear strain enhanced solid-shell element. The present formulation constitute an extension of the higher order shear deformation solid-shell finite element, developed by Hajlaoui et al. (2016), to the full nonlinear dynamics. The present solid-shell element formulation is based on the partition of shear strain: one of the parts is independent of the thickness coordinate and formulated by the Assumed Natural Strain (ANS) method, which avoids the shear locking in thin limit structure; the other enhancing part ensures a quadratic distribution across the thickness. With this shear strain enhancement, the accuracy of transverse shear stresses will be improved and the shear correction factors will be avoided.

The remainder of this paper is organized as follows. Functionally graded materials are described in section two. After that, solid-shell finite element formulation and a transient analysis of the nonlinear formulation is described in section three and four respectively. Numerical results and discussions of the finite element model are investigated in detail in section five. Finally, some concluding remarks are analyzed and presented in section six.

2 FUNCTIONALLY GRADED MATERIALS

In this paper, we consider an FGM shell structures made from a mixture of metal and ceramics and the composition varies continuously in the thickness direction. In fact, the Young's modulus $E(z)$, density $\rho(z)$ and Poisson's ratio $\nu(z)$ are assumed to vary through the shell thicknesses according to a power-law distribution as

$$E(z)=(E_c-E_m)V_c+E_m,\ \rho(z)=(\rho_c-\rho_m)V_c+\rho_m,\qquad \nu(z)=(\nu_c-\nu_m)V_c+\nu_m \tag{1}$$

in which the subscripts m and c refer to metal and ceramic components, respectively. In addition, the volume fraction V_c follows two general four-parameter power-law distributions, Su et al. (2014).

$$FGM_I(a,b,c,\mathrm{p}):\ V_c(z)=\left[1-a\left(\frac{1}{2}+\frac{z}{h}\right)+b\left(\frac{1}{2}+\frac{z}{h}\right)^c\right]^p \tag{2}$$

$$FGM_{II}(a,b,c,\mathrm{p}):\ V_c(z)=\left[1-a\left(\frac{1}{2}-\frac{z}{h}\right)+b\left(\frac{1}{2}-\frac{z}{h}\right)^c\right]^p \tag{3}$$

where a, b and c are the parameters which determine the material variation profile through the FGM shell thickness and p is the power-law index.

3 SOLID-SHELL FINITE ELEMENT FORMULATION

The developed solid-shell element is an eight nodes hexahedral element with three degrees of freedom per node. The transverse shear strain is composed of two parts. The first one is independent of the thickness coordinate and formulated by the assumed natural strain method (ANS). The second part is an enhancing part, which ensures a quadratic distribution through the thickness.

The enhanced assumed strain method consists in the enhancement of the compatible part of the Green Lagrange strain tensor, $\mathbf{E}^c$, with an enhanced part $\tilde{\mathbf{E}}$ to have a total strain as follows

$$\mathbf{E}=\mathbf{E}^c+\tilde{\mathbf{E}} \tag{4}$$

3.1 Variational Formulation

The point of departure is the well-known three-field variational functional in Lagrangean formulation. This variational functional is as follows

$$\Pi\left(\mathbf{u},\tilde{\mathbf{E}},\tilde{\mathbf{S}}\right)=\int_V\left[\psi\left(\mathbf{E}^c+\tilde{\mathbf{E}}\right)-\tilde{\mathbf{S}}:\tilde{\mathbf{E}}\right]dV-\int_V\mathbf{F}_V.\mathbf{u}dV-\int_{\partial V_f}\mathbf{F}_S.\mathbf{u}dA=0 \tag{5}$$

where ψ is the strain energy function and $\mathbf{u}$, $\tilde{\mathbf{E}}$ and $\tilde{\mathbf{S}}$ are the independent tonsorial quantities which are: displacement, enhanced assumed strain and assumed stress fields respectively. Also in Eq. (5) appear the prescribed body force $\mathbf{F}_V$ and surface traction $\mathbf{F}_S$. The orthogonality between the enhanced strain and stress fields leads to

$$\int_V\tilde{\mathbf{S}}:\tilde{\mathbf{E}}dV=0 \tag{6}$$

This orthogonality condition reduce the number of independent variables in the original functional to just two $\left(\mathbf{u},\tilde{\mathbf{E}}\right)$. The weak form of this modified reduced functional may be obtained with the direction derivative leading to

$$W\left(\mathbf{u},\tilde{\mathbf{E}}\right)=\delta\Pi=\int_V\mathbf{S}:\left(\delta\mathbf{E}^c+\delta\tilde{\mathbf{E}}\right)dV-\int_V\mathbf{F}_V.\delta\mathbf{u}dV-\int_{\partial V_f}\mathbf{F}_S.\delta\mathbf{u}dA=0 \tag{7}$$

where $\mathbf{S}$ is the Piola-Kirchhoff stress tensor

$$\mathbf{S}=\frac{\partial\psi}{\partial\mathbf{E}} \tag{8}$$

3.2 Finite Element Formulation

In each finite element domain, an eight-node hexahedral solid-shell element is considered. The position vectors in reference and current configurations respectively are

$$\mathbf{X}=\mathbf{N}\mathbf{X}_n\quad,\quad\mathbf{x}=\mathbf{N}\mathbf{x}_n \tag{9}$$

where $\mathbf{N}$ is the tri-linear shape functions matrix given by

$$\mathbf{N}=\begin{bmatrix}N_1\mathbf{I}_3 & N_2\mathbf{I}_3 & N_3\mathbf{I}_3 & N_4\mathbf{I}_3 & N_5\mathbf{I}_3 & N_6\mathbf{I}_3 & N_7\mathbf{I}_3 & N_8\mathbf{I}_3\end{bmatrix} \tag{10}$$

$\mathbf{x}_n$ and $\mathbf{X}_n$ are nodal coordinates. The displacement field, with the corresponding variation and increment, is interpolated in the same manner as follows

$$\mathbf{u}=\mathbf{N}\mathbf{U}_n\quad,\quad\delta\mathbf{u}=\mathbf{N}\delta\mathbf{U}_n\quad,\quad\Delta\mathbf{u}=\mathbf{N}\Delta\mathbf{U}_n \tag{11}$$

where $\mathbf{U}_n=\left[u_1,v_1,w_1,...u_8,v_8,w_8\right]^T$ is the nodal displacements vector at the element level. The covariant base vectors obtained by partial derivative of the position vectors with respect to convective coordinate $\boldsymbol{\xi}=\left(\xi_1,\xi_2,\xi_3\right)=\left(\xi,\eta,\zeta\right)$ in reference and current configuration are given by

$$\mathbf{G}_k=\frac{\partial\mathbf{X}}{\partial\xi_k},\qquad\mathbf{g}_k=\frac{\partial\mathbf{x}}{\partial\xi_k},k=1,2,3 \tag{12}$$

The covariant metric tensor at a material point $\boldsymbol{\xi}$, in the reference and current configuration are defined by

$$\mathbf{G} = \left[\mathbf{G}_i.\mathbf{G}_j\right] \quad , \quad \mathbf{g} = \left[\mathbf{g}_i.\mathbf{g}_j\right] \quad , \quad i,j = 1,2,3 \tag{13}$$

This leads to the following Green-Lagrangean strain tensor

$$\mathbf{E} = \frac{1}{2}\left(\mathbf{g} - \mathbf{G}\right) \quad , \quad E_{ij} = \frac{1}{2}\left(g_{ij} - G_{ij}\right) \tag{14}$$

3.3 Compatible Strains

To treat the transverse shear locking and transverse normal locking problems, the ANS method is used. For the transverse shear strains, E^c_{13} and E^c_{23}, the ANS method, proposed by Bathe and Dvorkin (1985), is used and evaluated at four mid-points of the element edges A = (-1,0,0), B = (0,-1,0), C = (1,0,0), D = (0,1,0), Fig. 1.

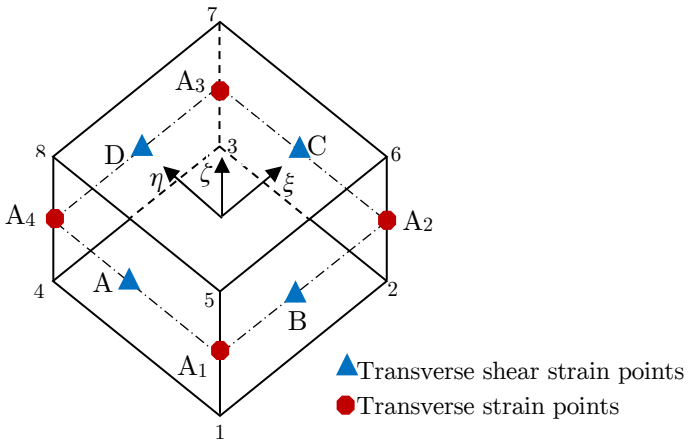

Figure 1: Transverse shear strain and thickness strain interpolation points.

The transverse shear strains are given by

$$\begin{bmatrix} E^c_{13} \\ E^c_{23} \end{bmatrix} = \frac{1}{2}\begin{bmatrix} \left(1-\eta\right)\left(g^B_{13} - G^B_{13}\right) + \left(1+\eta\right)\left(g^D_{13} - G^D_{13}\right) \\ \left(1-\xi\right)\left(g^A_{13} - G^A_{13}\right) + \left(1+\xi\right)\left(g^C_{13} - G^C_{13}\right) \end{bmatrix} \tag{15}$$

However, for the thickness strains, E^c_{33}, we adopt the ANS method as in Klinkel et al. (1999), Vu-Quoc and Tan (2003) and Hajlaoui et al. (2012, 2015, 2016) and evaluated at four collocation points defined in the reference surface $\left(\zeta = 0\right)$: A1=(-1,-1,0), A2=(1,-1,0), A3=(1,1,0), A4=(-1,1,0), Fig. 1. The thickness strains is given by

$$E_{33}^{c} = \sum_{L=1}^{4} \frac{1}{4}\left(1+\xi\xi_L\right)\left(1+\eta\eta_L\right)\frac{1}{2}\left(g_{33}^{L} - G_{33}^{L}\right) \tag{16}$$

For the detailed description of the ANS method, refer to Hajlaoui et al. (2012, 2015, 2016). The compatible part is arranged in (6x1) column matrix as follows

$$\mathbf{E}^{c} = \begin{bmatrix} E_{11}^{c} & E_{22}^{c} & E_{33}^{c} & 2E_{12}^{c} & 2E_{13}^{c} & 2E_{23}^{c} \end{bmatrix}^{T} \tag{17}$$

Using Eqs. (15)-(17) and approximations Eqs. (9) and (11), the virtual and incremental compatible Green Lagrange strain tensor are then given by

$$\delta\mathbf{E}^{c} = \mathbf{B}\,\delta\mathbf{U}_{n} \quad , \quad \Delta\mathbf{E}^{c} = \mathbf{B}\,\Delta\mathbf{U}_{n} \tag{18}$$

where $\mathbf{B}$ is the strain interpolation matrix, associated to node I $\left(I=1,8\right)$ and denoted $\mathbf{B}_I$ is given by

$$\mathbf{B}_I = \mathbf{T}^{-T}\begin{bmatrix} \mathbf{g}_1^{T}\,\mathrm{N}_{I,1} \\ \mathbf{g}_2^{T}\,\mathrm{N}_{I,2} \\ \sum_{L=1}^{4}\frac{1}{4}\left(1+\xi_L\xi\right)\left(1+\eta_L\eta\right)\mathbf{g}_3^{L^T}\,\mathrm{N}_{I,3}^{L} \\ \mathbf{g}_2^{T}\,\mathrm{N}_{I,1} + \mathbf{g}_1^{T}\,\mathrm{N}_{I,2} \\ \frac{1}{2}\left[\left(1-\eta\right)\left(\mathbf{g}_3^{B^T}\,\mathrm{N}_{I,1}^{B} + \mathbf{g}_1^{B^T}\,\mathrm{N}_{I,3}^{B}\right) + \left(1+\eta\right)\left(\mathbf{g}_3^{D^T}\,\mathrm{N}_{I,1}^{D} + \mathbf{g}_1^{D^T}\,\mathrm{N}_{I,3}^{D}\right)\right] \\ \frac{1}{2}\left[\left(1-\xi\right)\left(\mathbf{g}_3^{A^T}\,\mathrm{N}_{I,2}^{A} + \mathbf{g}_2^{A^T}\,\mathrm{N}_{I,3}^{A}\right) + \left(1+\xi\right)\left(\mathbf{g}_3^{C^T}\,\mathrm{N}_{I,2}^{C} + \mathbf{g}_2^{C^T}\,\mathrm{N}_{I,3}^{C}\right)\right] \end{bmatrix} \tag{19}$$

Matrix $\mathbf{T}$, in Eq. (19), is the transformation of the strain tensor from parametric coordinates to the local Cartesian coordinates, written as

$$\mathbf{T} = \begin{bmatrix} \left(t_{11}\right)^2 & \left(t_{21}\right)^2 & \left(t_{31}\right)^2 & 2t_{11}t_{21} & 2t_{11}t_{31} & 2t_{21}t_{31} \\ \left(t_{12}\right)^2 & \left(t_{22}\right)^2 & \left(t_{32}\right)^2 & 2t_{12}t_{22} & 2t_{12}t_{32} & 2t_{22}t_{32} \\ \left(t_{13}\right)^2 & \left(t_{23}\right)^2 & \left(t_{33}\right)^2 & 2t_{13}t_{23} & 2t_{13}t_{33} & 2t_{23}t_{33} \\ t_{11}t_{12} & t_{21}t_{22} & t_{31}t_{32} & t_{11}t_{22}+t_{12}t_{21} & t_{11}t_{32}+t_{12}t_{31} & t_{21}t_{32}+t_{22}t_{31} \\ t_{11}t_{13} & t_{21}t_{23} & t_{31}t_{33} & t_{11}t_{23}+t_{13}t_{21} & t_{11}t_{33}+t_{13}t_{31} & t_{21}t_{33}+t_{23}t_{31} \\ t_{12}t_{13} & t_{22}t_{23} & t_{32}t_{33} & t_{12}t_{23}+t_{13}t_{22} & t_{12}t_{33}+t_{13}t_{32} & t_{22}t_{33}+t_{23}t_{32} \end{bmatrix} \tag{20}$$

where $t_{ij} = \mathbf{G}_i.\mathbf{T}_j$ and $\mathbf{T}_j$ $(j = 1, 2, 3)$ are a local orthonormal base vectors.

3.4 Enhanced Strains

The enhanced Green-Lagrange strain part is related to the internal strain parameters vector $\boldsymbol{\alpha}$ as:

$$\tilde{\mathbf{E}} = \tilde{\mathbf{M}}\boldsymbol{\alpha}\,, \quad \delta\tilde{\mathbf{E}} = \tilde{\mathbf{M}}\delta\boldsymbol{\alpha} \quad , \Delta\tilde{\mathbf{E}} = \tilde{\mathbf{M}}\Delta\boldsymbol{\alpha} \tag{21}$$

where $\tilde{\mathbf{E}}$, $\delta\tilde{\mathbf{E}}$ and $\Delta\tilde{\mathbf{E}}$ are total, virtual and incremental enhanced Green Lagrange strain tensor respectively. The crucial assumption of the EAS method is the enforcement of the orthogonality conditions for the assumed stress field $\tilde{\mathbf{S}}$ and the enhanced strain $\tilde{\mathbf{E}}$. This orthogonality conditions impose the following choice for the interpolation function matrix $\tilde{\mathbf{M}}$ to be expressed as follows

$$\tilde{\mathbf{M}} = \frac{\det \mathbf{J}_0}{\det \mathbf{J}} \mathbf{T}_0^{-T} \mathbf{M}_{\xi\eta\zeta} \quad , \quad \int_{-1}^{1}\int_{-1}^{1}\int_{-1}^{1} \mathbf{M}_{\xi\eta\zeta} d\xi d\eta d\zeta = 0 \tag{22}$$

where the subscript '0' means the evaluation at the center of the element in the natural coordinates and $\mathbf{J} = \left[\mathbf{G}_1, \mathbf{G}_2, \mathbf{G}_3\right]$ is the Jacobian matrix. Eq. (22) responds a minimum requirement that the enhancing strain be orthogonal to the constant stress state. The interpolation matrix $\mathbf{M}_{\xi\eta\zeta}$, in Eq. (22), is expression in term of the parametric coordinates $\left(\xi, \eta, \zeta\right)$. Three choices of matrix $\mathbf{M}_{\xi\eta\zeta}$ can be considered with, 7, 9 and 11 parameters

$$\mathbf{M}_{\xi\eta\zeta}^{7} = \begin{pmatrix} \xi & 0 & 0 & 0 & 0 & 0 & 0 \\ 0 & \eta & 0 & 0 & 0 & 0 & 0 \\ 0 & 0 & \zeta & 0 & 0 & 0 & 0 \\ 0 & 0 & 0 & \xi & \eta & 0 & 0 \\ 0 & 0 & 0 & 0 & 0 & \frac{1}{5} - \zeta^2 & 0 \\ 0 & 0 & 0 & 0 & 0 & 0 & \frac{1}{5} - \zeta^2 \end{pmatrix} \tag{23.a}$$

$$\mathbf{M}_{\xi\eta\zeta}^{9} = \begin{pmatrix} \xi & 0 & 0 & 0 & 0 & 0 & 0 & 0 & 0 \\ 0 & \eta & 0 & 0 & 0 & 0 & 0 & 0 & 0 \\ 0 & 0 & \zeta & 0 & 0 & 0 & 0 & \xi\zeta & \eta\zeta \\ 0 & 0 & 0 & \xi & \eta & 0 & 0 & 0 & 0 \\ 0 & 0 & 0 & 0 & 0 & \frac{1}{5} - \zeta^2 & 0 & 0 & 0 \\ 0 & 0 & 0 & 0 & 0 & 0 & \frac{1}{5} - \zeta^2 & 0 & 0 \end{pmatrix} \tag{23.b}$$

$$\mathbf{M}_{\xi\eta\zeta}^{11} = \begin{pmatrix} \xi & 0 & 0 & 0 & 0 & 0 & 0 & 0 & 0 & \xi\eta & 0 \\ 0 & \eta & 0 & 0 & 0 & 0 & 0 & 0 & 0 & 0 & \xi\eta \\ 0 & 0 & \zeta & 0 & 0 & 0 & 0 & \xi\zeta & \eta\zeta & 0 & 0 \\ 0 & 0 & 0 & \xi & \eta & 0 & 0 & 0 & 0 & 0 & 0 \\ 0 & 0 & 0 & 0 & 0 & \frac{1}{5} - \zeta^2 & 0 & 0 & 0 & 0 & 0 \\ 0 & 0 & 0 & 0 & 0 & 0 & \frac{1}{5} - \zeta^2 & 0 & 0 & 0 & 0 \end{pmatrix} \tag{23.c}$$

In all these three matrices, the term $1/5 - \zeta^2$ ensures the parabolic transverse shear distribution in thickness direction. This enhancement requires a numerical integration rule at least 2x2x3. How-

ever, the three matrices are different in the plane and thickness strains enhancement. In a previous work, Hajlaoui et al. (2016), the analysis of stiffness matrix eigenvalue in the incompressible range demonstrate that only the 11 parameters solid shell element, Eq. (23.c), provided the correct eigenvalues. As FGM materials are far from incompressible conditions as in rubber or elastoplasticity, and to reduce the computational time, one can choose the nine parameters, C3D8C9 element, which will be the only considered in the numerical results.

3.5 Linearization

With the finite element approximation, Eq. (18) and (21), at hand, the continuum weak form, Eq. (7), became in a discrete form as

$$W = \delta \mathbf{U}_n^T \left(\mathbf{f}_{\text{int}} - \mathbf{f}_{ext} \right) + \delta \boldsymbol{\alpha}^T . \mathbf{h} \tag{24}$$

where, $\mathbf{f}_{\text{int}}$, $\mathbf{f}_{ext}$ and $\mathbf{h}$, are given by the following expressions

$$\mathbf{f}_{\text{int}} = \int_V \mathbf{B}^T \mathbf{S}\, dV \;\; , \;\; \mathbf{f}_{ext} = \int_V \mathbf{N}^T \mathbf{F}_V dV \; + \int_{\partial V_f} \mathbf{N}^T \mathbf{F}_S \text{dA} \;\; , \;\; \mathbf{h} = \int_V \tilde{\mathbf{M}}^T \mathbf{S}\, dV \tag{25}$$

Equation (24) is a nonlinear equation that will be solved iteratively by the Newton-Raphson method. For this purpose one need the corresponding linearization

$$W + DW.\left(\Delta \mathbf{U}_n, \Delta \boldsymbol{\alpha} \right) = \left[\delta \mathbf{U}_n^T \quad \delta \boldsymbol{\alpha}^T \right] \left(\begin{bmatrix} \mathbf{K} & \boldsymbol{L}^T \\ \boldsymbol{L} & \boldsymbol{H} \end{bmatrix} \begin{Bmatrix} \Delta \boldsymbol{U}_n \\ \Delta \boldsymbol{\alpha} \end{Bmatrix} + \begin{bmatrix} \mathbf{f}_{\text{int}} - \mathbf{f}_{ext} \\ \mathbf{h} \end{bmatrix} \right) = 0 \tag{26}$$

where $\mathbf{L}$, $\mathbf{H}$ and $\mathbf{K}$ are given by

$$\boldsymbol{L} = \int_V \tilde{\mathbf{M}}^T \mathcal{C}\, \boldsymbol{B}\, \text{dV} \,, \;\; \boldsymbol{H} = \int_V \tilde{\mathbf{M}}^T \mathcal{C}\, \tilde{\mathbf{M}}\, \text{dV} \;\; , \;\; \mathbf{K} = \mathbf{K}_D + \mathbf{K}_G \tag{27}$$

with $\mathcal{C} = \dfrac{\partial^2 \psi}{\partial \mathbf{E} \partial \mathbf{E}}$ is the 6×6 three dimensional material tangent moduli, or elasticity tensor, and $\mathbf{K}_D$ is given by

$$\mathbf{K}_D = \int_V \mathbf{B}^T \mathcal{C}\, \mathbf{B}\, dV \tag{28}$$

where the matrix $\mathbf{B}$ is given by Eq. (19) and $\mathbf{K}_G$ is the geometric stiffness matrix

$$\delta \mathbf{U}_n^T \mathbf{K}_G \Delta \mathbf{U}_n^T = \int_V \mathbf{S}^T \Delta \delta \mathbf{E}^{\mathbf{c}} dV \tag{29}$$

Relative to a couple of nodes (I, J) the matrix $\mathbf{K}_G$ is given by

$$\mathbf{K}_G^{IJ} = \int_V diag\begin{bmatrix} G_{IJ} & G_{IJ} & G_{IJ} \end{bmatrix} dV \tag{30}$$

$$G_{IJ} = \mathbf{S}^T\mathbf{T}^{-T}\begin{bmatrix} \mathrm{N}_{I,1}\,\mathrm{N}_{J,1} \\ \mathrm{N}_{I,2}\,\mathrm{N}_{J,2} \\ \sum_{L=1}^{4}\frac{1}{4}\big(1+\xi_L\xi\big)\big(1+\eta_L\eta\big)\mathrm{N}^L_{I,3}\,\mathrm{N}^L_{J,3} \\ \mathrm{N}_{I,1}\,\mathrm{N}_{J,2}+\mathrm{N}_{I,2}\,\mathrm{N}_{J,1} \\ \frac{1}{2}\Big[\big(1-\eta\big)\big(\mathrm{N}^B_{I,1}\,\mathrm{N}^B_{J,3}+\mathrm{N}^B_{I,3}\,\mathrm{N}^B_{J,1}\big)+\big(1+\eta\big)\big(\mathrm{N}^D_{I,1}\,\mathrm{N}^D_{J,3}+\mathrm{N}^D_{I,3}\,\mathrm{N}^D_{J,1}\big)\Big] \\ \frac{1}{2}\Big[\big(1-\xi\big)\big(\mathrm{N}^A_{I,2}\,\mathrm{N}^A_{J,3}+\mathrm{N}^A_{I,3}\,\mathrm{N}^A_{J,2}\big)+\big(1+\xi\big)\big(\mathrm{N}^C_{I,2}\,\mathrm{N}^C_{J,3}+\mathrm{N}^C_{I,3}\,\mathrm{N}^C_{J,2}\big)\Big] \end{bmatrix} \tag{31}$$

The strain parameters $\Delta\boldsymbol{\alpha}$ must be eliminated from Eq. (26) at the element level, which leads to following element tangent operator $\mathbf{K}_T$ and residual vector $\mathbf{R}$

$$\mathbf{K}_T = \Big(\mathbf{K}_D - \boldsymbol{L}^T\boldsymbol{H}^{-1}\boldsymbol{L}\Big) + \mathbf{K}_G \quad , \qquad \mathbf{R} = \boldsymbol{L}^T\boldsymbol{H}^{-1}\boldsymbol{h} + \mathbf{f}_{ext} - \mathbf{f}_{\mathrm{int}} \tag{32}$$

4 TRANSIENT ANALYSIS OF THE NON-LINEAR FORMULATION

In order to extend the variational formulation, Eq. (24), to accommodate transient analysis, the body force is replaced by $\mathbf{F}_V \leftarrow \mathbf{F}_V - \rho\ddot{\mathbf{u}}$. Then, with this replacement the variational equation became

$$W = \delta\mathbf{U}_n^T\left(\mathbf{f}_{\mathrm{int}} + \mathbf{f}_{\mathrm{iner}} - \mathbf{f}_{ext}\right) + \delta\boldsymbol{\alpha}^T.\mathbf{h} \quad , \ \mathbf{f}^e_{iner} = \int_V \mathbf{N}^T\rho\ddot{\mathbf{u}}\,dV \tag{33}$$

The acceleration in Eq. (33) is computed from the isoparametric interpolation as in Eq. (11). Thus, the inertia term and residual vector may be written as

$$\mathbf{f}_{iner} = \mathbf{M}\ddot{\mathbf{U}}_n \quad , \qquad \mathbf{R} = \mathbf{f}_{ext} - \mathbf{f}_{\mathrm{int}} + \boldsymbol{L}^T\boldsymbol{H}^{-1}\boldsymbol{h} - \mathbf{M}\ddot{\mathbf{U}}_n \tag{34}$$

where $\mathbf{M}$ is the consistent mass matrix. The Newmark method is a one-step method, which is used to advance the solution from time t_n to t_{n+1}. Firstly, given the initial displacement and velocity vectors, the initial acceleration is determined by solving Eq. (34). The Newmark formula to process the solution is given by

$$\mathbf{K}^*_T\Delta\mathbf{U}^{i+1}_{n+1} = \mathbf{R}^i_{n+1} \quad , \qquad \mathbf{K}^*_T = \mathbf{K}_T + \frac{\gamma}{\beta\Delta t}\mathbf{C}_T + \frac{1}{\beta\Delta t^2}\mathbf{M} \tag{35}$$

with the updating formulas

$$\mathbf{U}^{i+1}_{n+1} = \mathbf{U}^i_{n+1} + \Delta\mathbf{U}^{i+1}_{n+1}, \dot{\mathbf{U}}^{i+1}_{n+1} = \dot{\mathbf{U}}^i_{n+1} + \frac{\gamma}{\beta\Delta t}\Delta\mathbf{U}^{i+1}_{n+1}, \quad \ddot{\mathbf{U}}^{i+1}_{n+1} = \ddot{\mathbf{U}}^i_{n+1} + \frac{1}{\beta\Delta t^2}\Delta\mathbf{U}^{i+1}_{n+1} \tag{36}$$

where $\mathbf{U}^{i+1}_{n+1}$, $\dot{\mathbf{U}}^{i+1}_{n+1}$, and $\ddot{\mathbf{U}}^{i+1}_{n+1}$ are displacement, velocity and acceleration vectors given in the initial state by

$$\mathbf{U}^0_{n+1} = \mathbf{U}_n \ , \quad \dot{\mathbf{U}}^0_{n+1} = \left(1-\frac{\gamma}{\beta}\right)\dot{\mathbf{U}}_n + \Delta t\left(1-\frac{\gamma}{2\beta}\right)\ddot{\mathbf{U}}_n \quad , \quad \ddot{\mathbf{U}}^0_{n+1} = -\frac{1}{2\beta}\dot{\mathbf{U}}_n + \left(1-\frac{1}{2\beta}\right)\ddot{\mathbf{U}}_n \tag{37}$$

The Newmark parameters β and γ are chosen as $\beta = 0.25$, $\gamma = 0.5$.

5 NUMERICAL RESULTS AND DISCUSSION

The finite element formulation of the present higher order shear strain enhanced solid-shell element for nonlinear dynamic analyses of functionally graded material shell structures as presented in the previous sections. In this section, a comprehensive investigation concerning the nonlinear dynamic response of functionally graded material shell structures with various boundary conditions is given to demonstrate the accuracy and reliability of the present higher order solid-shell element.

5.1 Pull-Out of an Open-Ended Isotropic Cylindrical Shell

The purpose of this example is to demonstrate the ability of the formulation to capture large displacement and illustrate the robustness of the numerical implementation in static analysis. A short cylinder, with two pinching vertical forces at the middle section is modeled using one octant Fig. 2a.

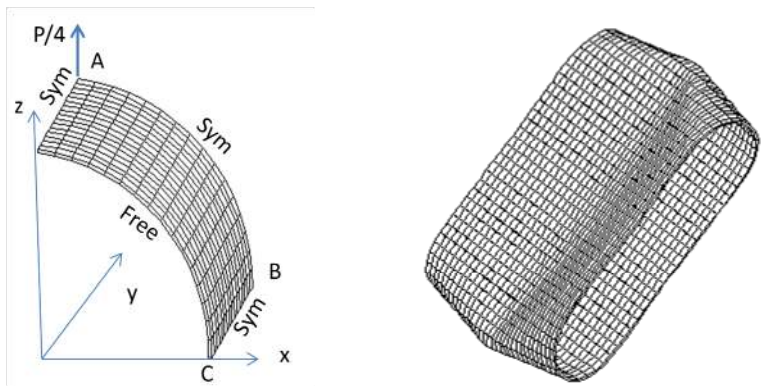

a/ b/

Figure 2: Pull-out of an open-ended cylindrical shell a/ Finite element model, b/ Reel deformed configuration at P=40000.

This popular benchmark problem constitutes a severe test of shell finite element formulations and has been addressed in Sze et al. (2004) and Payette and Reddy (2014) among others. A 16x16 meshing is used for this validation test and applying the appropriate symmetry boundary conditions, Fig. 2.a. The length of the cylinder is L=10.35, the radius is R=4.953, and the thickness is h= 0.094. Material properties for this test are $E = 10.5 \times 10^6$, $\nu = 0.3125$. The concentrated load P=*40000* is applied at point A. The automatic incremental/iterative Newton procedure is used with a total of 64 load steps. The final reel deformed configuration is given at Fig. 2.b. The radial deflections vs. the net applied pulling force P are shown in Fig. 3 for points A, B and C.

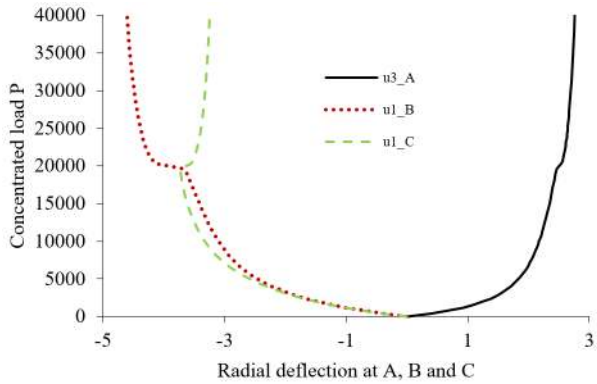

Figure 3: Pull-out force P vs. radial deflections at points A, B and C for the open-ended cylindrical shell.

The results shown in Figs. 3 are visually in unison with radial deflections for points A, B and C provided by Payette and Reddy (2014).

5.2. Shallow Spherical Cap Under a Concentrated Load

In this sub-section, we present numerical simulations in order to illustrate the good performance of the proposed formulation. The dynamic behavior of a clamped isotropic spherical shell under a concentrated apex load, *F=100*, is presented. This test is proposed in Duarte Filho and Awruch (2004). Material and geometric properties for this test are $E = 10^7$, $\nu = 0.3$, $\rho = 0.000245$, $\theta = 10.9°$, *R=4.76*, and $h = 0.01576$. Loading and finite element mesh are shown in Fig.4.

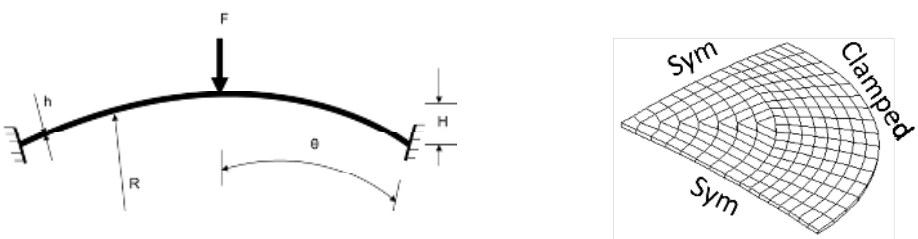

Figure 4: Shallow spherical cap, geometry and finite element modeling.

The time increment is $\Delta t = 0.2\mu s$ and the finite element mesh with 192 elements is used. The nonlinear dynamic response, represented by the vertical displacement at the mid-span, is shown in Fig 5. In the same figure, results obtained from a nonlinear and linear static analyses, as well as the linear dynamic analysis are presented. These results are compared with the results of Duarte Filho and Awruch (2004). The proposed formulation presents a very close results to Duarte Filho and Awruch (2004) results.

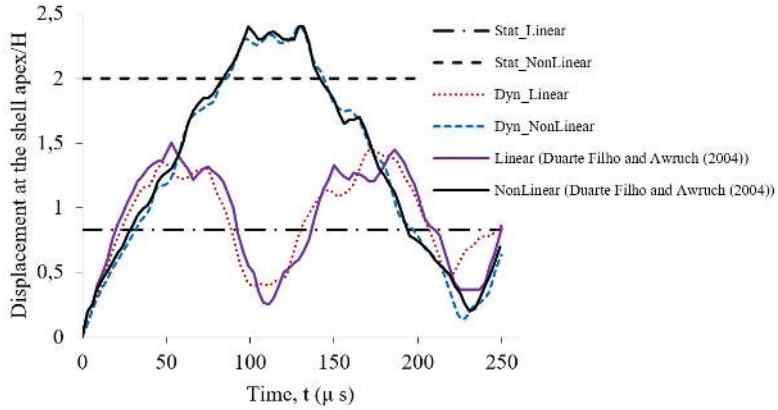

Figure 5: Dynamic response of the isotropic shallow spherical cap.

5.3 FGM Plate Under Constant Distributed Load

This example consists on a square functionally graded plate subjected to a constant uniformly distributed loading of $q = -10^6 N / m^2$. This numerical test has been addressed in Praveen and Reddy (1998) among others. The side length or the plate is $a=b=0.2m$ and the thickness $h = 0.01m$.

The plate is made of the constituent materials: aluminum (bottom surface) and zirconia (top surface). Young's modulus, Poisson's ratio and density for the aluminum are $E_m = 70\ GPa$, $\nu = 0.3$, $\rho = 2707\ kg / m^3$, and for zirconia are $E_c = 151\ GPa$, $\nu = 0.3$, $\rho = 3000\ kg / m^3$, respectively. The used law distribution of the FGM plate is the classical power-law which can be obtained by the general four-parameter power-law distribution Eq. (3): $FGM_{II}\left(1,0,c,\mathrm{p}\right)$. By noting the symmetry, only one quadrant of the plate is modeled with 8x8x1 elements. The time increment is $\Delta t = 10^{-5} s$. The center deflection and time were non-dimensionalized according to the following expressions: center deflection $\overline{w} = w E_m h / \left(q a^2\right)$ and time $\overline{t} = t\sqrt{E_m / \left(a^2 \rho_m\right)}$.

Figs. 6 and 7 show the dynamic response of the Aluminum-Zirconia plates simply supported and clamped boundary conditions respectively. The accuracy of the present model is verified by comparing the computed non-dimensionalized center deflection with available results of Praveen and Reddy (1998). It is clear that the presently computed non-dimensionalized center deflection is in general in good agreement with Praveen and Reddy (1998) finite element solutions. However, a discrepancy exists for a higher magnitude of deflection in the simply supported plate, Fig.6. This can be explained by the major difference between the present formulation and Praveen and Reddy (1998): the present formulation is full 3D enhanced Green-Lagrange formulation and Praveen and Reddy (1998) is a 2D FSDT of plate with PSA and von-Karman nonlinearity.

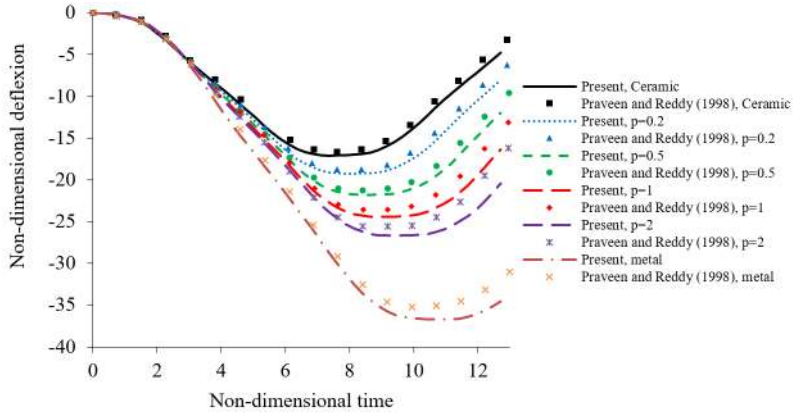

Figure 6: Temporal evolution of center deflection of simply supported FGM square plates under suddenly applied uniform load.

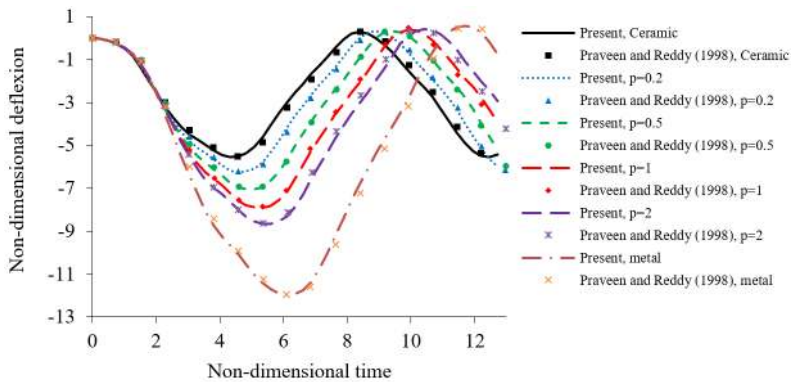

Figure 7: Temporal evolution of center deflection of clamped FGM square plates under suddenly applied uniform load.

5.4 Clamped Circular FGM Plate Under Distributed Transverse Load

This example, investigated in Nguyen and Nguyen-Xuan (2015), consists on clamped circular FGM plates under uniform pressure 10^6 N/m^2. The radius is R=0.5 m and the thickness is h=0.1 m. The circular FGM plate is made of the same constituent materials as the previous example, Aluminum-Zirconia. The used law distribution of the FGM plate is the classical power-law which can be obtained by the general four-parameter power-law distribution Eq. (3): $FGM_{II}\left(1,0,c,\mathrm{p}\right)$. Using symmetry boundary conditions, one quadrant of the shell is modeled with 192 elements, Fig. 8. A time step of 10^{-5} s is used in this problem. The center deflection and time were non-dimensionalized according to the following expressions: center deflection $\overline{w} = w.E_m h \,/\, \left(q\, R^2\right)$ and time $\overline{t} = t\sqrt{E_m \,/\, \left(R^2 \rho_m\right)}$.

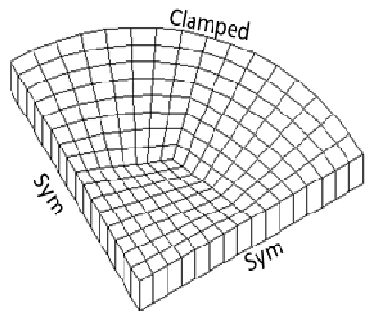

Figure 8: A quadrant of the clamped FGM circular plate modeled by 192 elements, 434 nodes.

Fig. 9 illustrates the central deflection dynamic response of the clamped FGM circular plate. In this figure, ANSYS solutions, for full metal and full ceramic, using quadratic finite elements and approximately 140436 degrees of freedom, are given in Nguyen and Nguyen-Xuan (2015). The present solutions, using only 1302 degrees of freedom, match very well with the ones obtained using ANSYS software. In addition, Fig. 9 shows the results obtained using several values of the power low index, 0.2, 0.5, 1 and 2. The present results are in good agreement with the published ones given in Nguyen and Nguyen-Xuan (2015) using 2535 degrees of freedom.

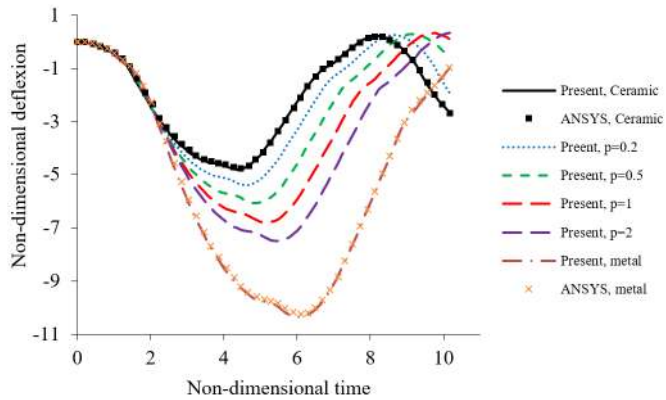

Figure 9: Temporal evolution of center deflection of clamped FGM circular plate under suddenly applied uniform load.

5.5 Simply Supported FGM Plate Under Varying Distributed Load

This numerical example consist on a simply supported square functionally graded plate of side length $a=b=1m$ and thickness $h = 0.01\ m$. The FGM plate is subjected to a uniformly distributed excited transverse load $q(t) = N\sin(\Omega t)$. The FGM plate is made of the constituent materials: aluminum (bottom surface) and alumina (top surface). Young's modulus, Poisson's ratio and density for the aluminum are $E_m = 70\ GPa$, $\nu_m = 0.3$ and $\rho_m = 2707\ kg/m^3$ and for alumina are

$E_c = 380\ GPa$, $\nu_c = 0.3$ and $\rho_c = 3800\ kg/m^3$, respectively. The used law distribution of the FGM plate is the classical power-law which can be obtained by the general four-parameter power-law distribution Eq. (3): $FGM_{II}\left(1,0,c,\mathrm{p}\right)$. This numerical problem is investigated in Duc and Cong (2015) with a sigmoid-FGM material. By noting the symmetry, only one quadrant of the plate is modeled with 8 x 8 x 1 elements. A time step of 10^{-3} s is used in this numerical test.

Fig. 10.a shows the nonlinear dynamic response, represented by graph of maximum deflection (p=1, N=1500N/m^2, Ω= 500). In the same conditions Fig. 10.b shows the relation of maximum deflection and the velocity of maximum deflection.

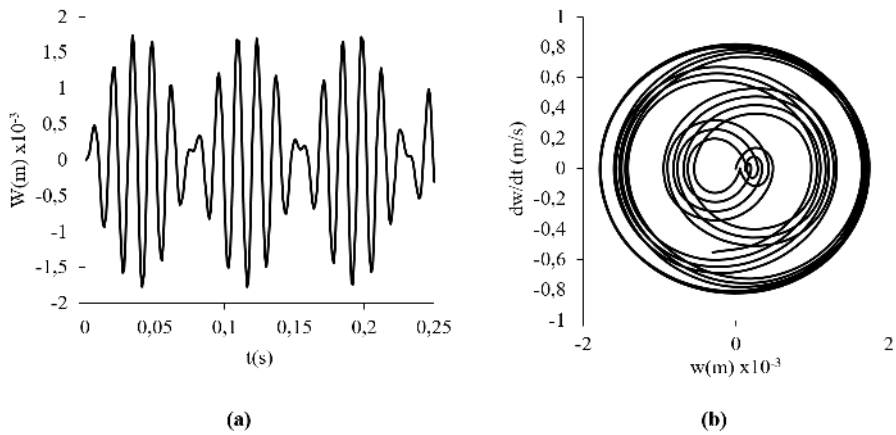

Figure 10: Nonlinear dynamic response of the square FGM plate (a) maximum deflection versus time (b) velocity versus maximum deflection.

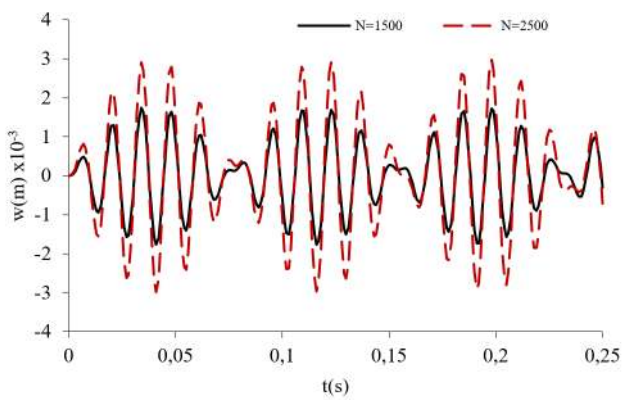

Figure 11: Nonlinear dynamic response of the square FGM plate under different loads.

Fig.11 shows the nonlinear response of the FGM square plate with different intensity of loads: N=1500N/m^2 and N=2500N/m^2; Ω= 500, p=1. From obtained results, one can see that amplitudes increase, when increasing the intensity of loads. The non-linear transient responses perform the phenomenon like periodic cycles.

Figure 12 shows the nonlinear response of the FGM square plate with different power-law index: p=1, p=2 and p=3; N=1500N/m^2, Ω= 500. From obtained results, one can see that amplitudes decrease, when increasing the power law index. This is because the plate is stiffened due to increasing the volume fraction index of the ceramic phase. The non-linear transient responses perform the phenomenon like periodic cycles.

The results shown in Figs. 10, 11 and 12 are visually in unison with those provided by Duc and Cong (2015) using a sigmoid distribution instead of the present power low distribution.

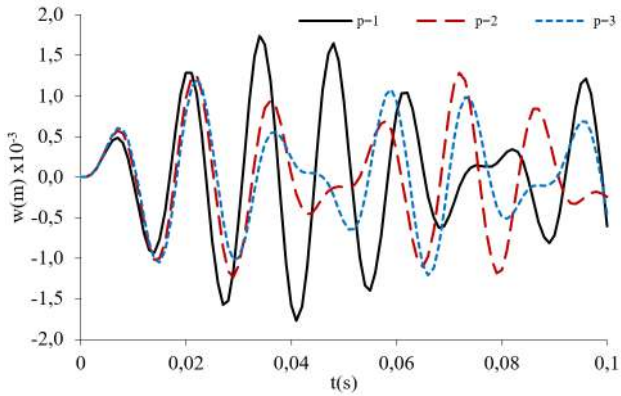

Figure 12: Nonlinear dynamic response of the square FGM plate under different power-law index.

5.6 Non-Linear Dynamic Analyses of FGM Cylindrical Shells

This numerical example, examined in Bich and Nguyen (2012), consist on an FGM cylindrical shell with radius of curvature R, thickness h and length L subjected to an external pressure uniformly distributed on the surface of the shell $q(t) = N\sin(\Omega t)$. Suppose that the material composition of the shell varies following a simple power law in terms of the volume fractions which can be deduced by the general four-parameter power-law distribution $FGM_{II}\left(1,0,c,\mathrm{p}\right)$. We consider the FGM cylindrical shells composed of ZrO2 and Ti–6Al–4V with the material properties for ZrO2: $E_c = 154.3211\ GPa$, $\rho_c = 5700\ kg\ /\ m^3$, $\nu_c = 0.298$ and for Ti–6Al–4V: $E_m = 105.6960\ GPa$, $\rho_m = 4429\ kg\ /\ m^3$, $\nu_m = 0.2981$. Simply supported boundary conditions are considered at $x = 0$ and $x = L$. By noting the symmetry, only one octant of the cylindrical shell is modeled with 16x16x1 elements.

Fig. 13 illustrate the effect of the power law index p on the nonlinear dynamic response of ZrO2/Ti–6Al–4V FGM cylindrical shells with $L\ /\ R = 2$, $R\ /\ h = 500$ and $q(t) = 1500\sin(600t)$. As remarked in previous test, the amplitude of the nonlinear dynamic of the FGM shells increases when increasing the power low index p.

Fig. 14 gives the effect of the thickness ration R/h on the nonlinear response of FGM cylindrical shell with $L\ /\ R = 2$, $p = 2$ and $q(t) = 1500\sin(600t)$. As had been anticipated, the amplitude of the FGM cylindrical shells increase when the ration R/h increase.

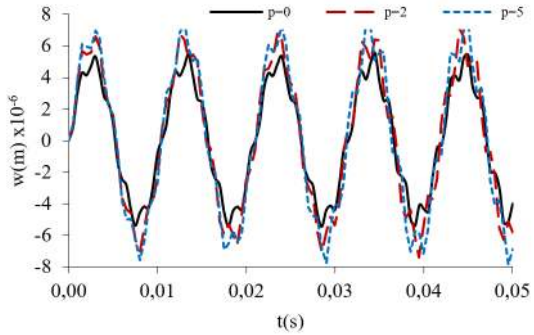

Figure 13: Effect of power law index p on the responses of FGM cylindrical shell.

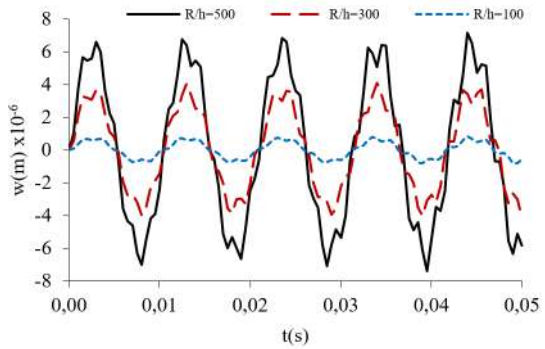

Figure 14: Effect of ratio R/h on the responses of FGM cylindrical shell.

6 CONCLUSION

This paper presents a numerical investigation on the nonlinear dynamic response of FGM shell structures. Material properties of the shell structure are assumed to vary continuously through the thickness according to the general four-parameter power-law distribution in terms of the volume fractions of the constituents.

The finite element formulation is based on the higher order shear strain enhanced solid-shell element. To avoid locking in the thin shell cases, the ANS method, for the transverse shear strains and thickness strain, is used instead of the continuum components in the compatible part of strain tensor. In the enhanced strain part, parabolic functions in terms of natural thickness coordinate are considered for the transverse shear strains. This permit to remove shear correction factors and improves the accuracy of transverse shear stresses. In addition, the enhancements of membrane part and the transverse strain are considered to avoid the in-plane bending and volumetric locking.

In the present solid-shell element, the nonlinear dynamics of FGM shell is done by the linearization of the nonlinear dynamic weak form. This was performed for use in the iterative solution for the kinematics quantities via the Newton's method. A time stepping algorithm based on the Newmark's scheme is employed in our time discrete weak form. From a demonstrative numerical simulation of complex FGM structures, it is found that the proposed method shows accurate results with good convergence characteristics.

Results of the present formulations are verified by comparing the present results with those available in literatures. The obtained results show the effects of material, boundary conditions, excitation and geometrical parameters on the dynamical response of FGM structures. Thus, it is obvious that the dynamic response of the considered FGM structures depends on many factors significantly: power low index, boundary conditions, excitation and geometrical parameters of the FGM structures.

In addition, the present higher order solid-shell model can be used in complex FGM or composite shell's structures analysis, unlike the analytic formulation that can be employed only for smooth differentiable geometry of shell structures.

References

Alijani, F., Amabili, M., Karagiozis, K., Bakhtiari-Nejad, F., (2011). Nonlinear vibrations of functionally graded doubly curved shallow shells. Journal of Sound and Vibration 330:1432-1454.

Allahverdizadeh, A., Naei, MH., Nikkhah Bahrami, M., (2008). Nonlinear free and forced vibration analysis of thin circular functionally graded plates. Journal of Sound and Vibration 310:966-984.

Ansari, R., Hasrati, E., Shojaei, M. F., Gholami, R., Mohammadi, V., Shahabodini, A., (2016). Size-Dependent Bending, Buckling and Free Vibration Analyses of Microscale Functionally Graded Mindlin Plates Based on the Strain Gradient Elasticity Theory. Latin American Journal of Solids and Structures 13: 632-664

Asemi, K., Salami, S.J., Salehi, M., Sadighi, M., (2014). Dynamic and Static analysis of FGM Skew plates with 3D Elasticity based Graded Finite element Modeling. Latin American journal of Solids and Structures 11:504-533.

Bathe, K.J., Dvorkin, E., (1985). A four-node plate bending element based on Mindlin/Reissner plate theory and a mixed interpolation. International Journal for Numerical Methods in Engineering 21:367-383.

Bich, DH., Nguyen, N.X., (2012). Nonlinear vibration of functionally graded circular cylindrical shells based on improved Donnell equations. Journal of Sound and Vibration 331:5488-5501.

Dammak, F., Abid, S., Gakwaya, A., Dhatt, G., (2005). A formulation of the non linear discrete Kirchhoff quadrilateral shell element with finite rotations and enhanced strains. Revue Européenne des Eléments Finis 14:7-31.

Duarte Filho, L.A., Awruch, A.M., (2004). Geometrically nonlinear static and dynamic analysis of shells and plates using the eight-node hexahedral element with one-point quadrature. Finite Elements in Analysis and Design 40:1297-1315.

Duc, N.D., (2013). Nonlinear dynamic response of imperfect eccentrically stiffened FGM double curved shallow shells on elastic foundation. Composite Structures 99:88-96.

Duc, N.D., Cong, P.H., (2015). Nonlinear dynamic response of imperfect symmetric thin sigmoid-functionally graded material plate with metal-ceramic-metal layers on elastic foundation. Journal of Vibration and Control 21:637-646.

Duc, N.D., Tuan, N.D., Tuan, P., Dao, N.T., Dat, N.T., (2015). Nonlinear dynamic analysis of sigmoid functionally graded circular cylindrical shells on elastic foundations using the third order shear deformation theory in thermal environments. International Journal of Mechanical Sciences 101-102:338-348.

Frikha, A., Dammak, F., (2017). Geometrically non-linear static analysis of functionally graded material shells with discrete double directors shell element. Computer Methods in Applied Mechanics and Engineering. 315:1-24.

Frikha, A., Wali, M., Hajlaoui, A., Dammak, F., (2016). Dynamic response of functionally graded material shells with a discrete double directors shell element. Composite Structures 154 :385–395.

Gharooni, H., Ghannad, M., (2015). Elastic analysis of pressurized thick FGM cylinders with exponential variation of material properties using TSDT. Latin American Journal of Solids and Structures 12 (6):1024-1041

Hajlaoui, A., Jarraya, A., El Bikri, K., Dammak, F., (2015). Buckling analysis of functionally graded materials structures with enhanced solid-shell elements and transverse shear correction. Composite Structures 132:87-97.

Hajlaoui, A., Jarraya, A., Kallel-Kammoun, I., Dammak, F., (2012). Buckling analysis of a laminated composite plate with delaminations using the enhanced assumed strain solid shell element. Journal of Mechanical Science and Technology, 26:3213-3221.

Hajlaoui, A., Wali, M., Ben Jdidia, M., Dammak, F., (2016). An improved Enhanced Solid Shell Element for Static and Buckling Analysis of shell structures, Mechanics & Industry, 17:510.

Hao, Y.X., Chen, L.H., Zhang, W., Lei, J.G., (2008). Nonlinear oscillations, bifurcations and chaos of functionally graded materials plate. Journal of Sound and Vibration 312:862-892.

Kadoli, R., Ganesan, N., (2006). Buckling and free vibration analysis of functionally graded cylindrical shells subjected to a temperature-specified boundary condition. Journal of Sound and Vibration 289:450-480.

Klinkel, S., Gruttmann, F., Wagner, W., (1999). A continuum based three-dimensional shell element for laminated structures. Computers & Structures 71:43-62.

Liew, K.M., Yang, J., Wu, Y.F., (2006). Nonlinear vibration of a coating-FGM-substrate cylindrical panel subjected to a temperature gradient. Computer Methods in Applied Mechanics and Engineering 195:1007-1026.

Liu, Y.Z., Hao, Y.X., Zhang, W., Chen, J., Li, S.B., (2015). Nonlinear dynamics of initially imperfect functionally graded circular cylindrical shell under complex loads. Journal of Sound and Vibration 348:294-328.

Nguyen, K.D., Nguyen-Xuan, H., (2015). An isogeometric finite element approach for three-dimensional static and dynamic analysis of functionally graded material plate structures. Composite Structures 132:423-439

Payette, G.S., Reddy, J.N., (2014). A seven-parameter spectral/hp finite element formulation for isotropic, laminated composite and functionally graded shell structures. Computer methods in applied mechanics and engineering 278:664-704.

Praveen, G.N., Reddy, J.N., (1998). Nonlinear transient thermoelastic analysis of functionally graded ceramic-metal plates. International Journal of Solids and Structures 35:4457-4476.

Reddy, J.N., (2000). Analysis of functionally graded plates. International Journal for Numerical Methods in Engineering 47:663-684.

Su, Z., Jin, G., Shi, S., Ye, T., Jia, X., (2014). A unified solution for vibration analysis of functionally graded cylindrical, conical shells and annular plates with general boundary conditions. International Journal of Mechanical Sciences 80:62-80.

Sze, K.Y., Liu, X.H., Lo, S.H., (2004). Popular benchmark problems for geometric nonlinear analysis of shells. Finite Elements in Analysis and Design 40:1551-1569.

Vel, SS., Batra, RC., (2004). Three dimensional exact solution for the vibration of FGM rectangular plates. Journal of Sound and Vibration 272:703-730.

Vu-Quoc, L., Tan, X.G., (2003). Optimal solid shells for non-linear analyses of multilayer composites. I. Statics. Computer methods in applied mechanics and engineering 192:975-1016.

Wali, M., Hajlaoui, A., Dammak, F., (2014). Discrete double directors shell element for the functionally graded material shell structures analysis. Computer Methods in Applied Mechanics and Engineering 278:388-403.

Wali, M., Hentati, T., Jarraya, A., Dammak, F., (2015). Free vibration analysis of FGM shell structures with a discrete double directors shell element. Composite Structures 125:295-303.

Woo, J., Meguid, SA., Ong, LS., (2006). Nonlinear free vibration behavior of functionally graded plates. Journal of Sound and Vibration 289:595-611.

Yang, J., Shen, H.S., (2002). Vibration characteristic and transient response of shear-deformable functionally graded plates in thermal environments, Journal of Sound and Vibration, 255:579-602.

Zhang, W., Hao, Y.X., Yang, J., (2012). Nonlinear dynamics of FGM circular cylindrical shell with clamped–clamped edges. Composite Structures 94:1075-1086.

Zhi-Yuan, C., Hua-Ning, W., (2007). Free vibration of FGM cylindrical shells with holes under various boundary conditions. Journal of Sound and Vibration 306:227-237.